arXiv:1702.05650v1 [cs.CV] 18 Feb 2017

Revisiting Graph Construction for Fast Image Segmentation

Zizhao Zhang, Fuyong Xing, Xiaoshuang Shi, Lin Yang
University of Florida
zizhao@cise.ufl.edu, {f.xing,xsshi2015}@ufl.edu, lin.yang@bme.ufl.edu

Abstract

In this paper, we propose a simple but effective method for fast image segmentation. We re-examine the locality-preserving character of spectral clustering by constructing a graph over image regions with both global and local connections. Our novel approach to build graph connections relies on two key observations: 1) local region pairs that co-occur frequently will have a high probability to reside on a common object; 2) spatially distant regions in a common object often exhibit similar visual saliency, which implies their neighborship in a manifold. We present a novel energy function to efficiently conduct graph partitioning. Based on multiple high quality partitions, we show that the generated eigenvector histogram based representation can automatically drive effective unary potentials for a hierarchical random field model to produce multi-class segmentation. Sufficient experiments on the BSDS500 benchmark demonstrate the competitive segmentation accuracy and significantly improved efficiency of our proposed method compared with other state of the arts.

1. Introduction

Image segmentation is a challenging and critical computer vision task. Graph-based algorithms have been shown as an effective approach for image segmentation [1, 2]. Among various graph based approaches, spectral clustering becomes a major trend [3].

Recent methods attempt to solve several primary issues of spectral clustering (referring to normalized cuts (NCut) [4]) based image segmentation. First, NCut based methods tend to segment image into spatially connected components [4, 5]. Multiscaling processing [6, 7] is a common way to address this problem by building the affinity for distant pixel affinities [8, 7], but most current cutting-edge methods do not follow this line. Instead, recent methods, like gPb [9] and MCG [10, 5] based methods [11] use the boundary-preserving property of NCut to trace boundary orientation information rather than the direct segmentation. Building effective affinity matrices [5, 3, 10] usually use sophisticated low-level features [9]. These features can effectively measure the local changes but are not effective in capturing high-level knowledge for segmentation. They are not good options for fast segmentation either. Different from previous approaches, our method re-examines spectral clustering from a manifold learning perspective to construct a graph to model the high-level image knowledge (i.e., pixel pair co-occurrence and saliency relationship) for unsupervised image segmentation. More importantly, our method provides the possibility of enabling graph partitioning to directly segment challenging natural images rather than just boundary tracing.

To better illustrate the motivation, we first explain the latent relation of NCut to manifold learning. Both NCut and Laplacian eigenmaps [12] take advantage of the locality-preserving character [13] of graph Laplacian to conduct clustering and dimensionality reduction. In fact, locality-based dimensionality reduction methods are implicitly tied to clustering [12]. Preserving locality is the key factor that drives effective clustering. Let's assume pixels of an image lie on a certain manifold where pixels belonging to a common object are adjacent (within a small range), but far away in the spatial image plane. These pixels supposed to have strong connections to be grouped together, but these connections are not encoded in the sparse affinity matrix of NCut due to their Euclidean distances. Although multi-scale affinity matrices [6, 8] can alleviate this issue, they are not essentially the solution to encode useful high-level knowledge for more effective graph construction as the proposed method emphasizes.

In this paper, we propose a novel approach to construct an image region graph to address the aforementioned problems. The overall idea is illustrated in Figure 1. The graph nodes are connected among both spatially adjacent and distant regions through different and independent cues. We build local connections between spatially adjacent regions with an affinity matrix. The estimation of the similarity between two regions is based on an observation that adjacent region pairs co-occurring frequently often reside on a common object. Oppositely, global connections are built among adjacent regions in the manifold which might be spatially

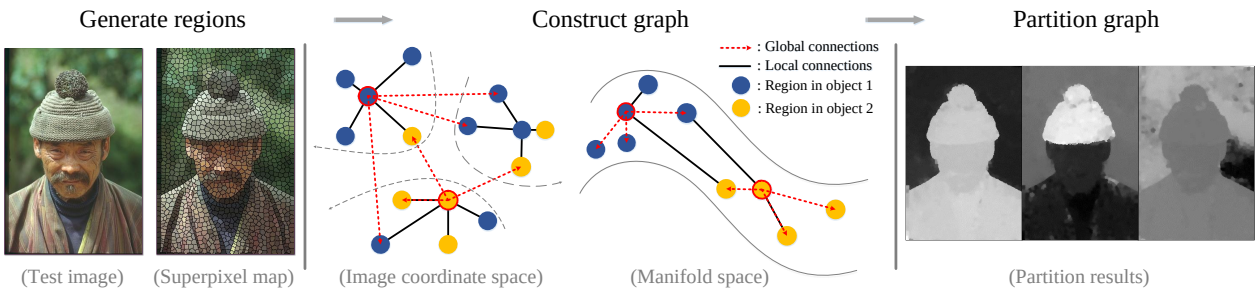

Figure 1: Illustration of the graph construction and partition procedures. The test image is first divided into over-segmented regions (left). Each region is treated as a graph node (middle). Local connections (black solid lines) link each region to its spatially adjacent regions in the image plane. When viewing those regions in a certain manifold space, spatially distant regions in the same object will be adjacent; directed global connections (red dotted arrows) link each region to its neighbors. We cut the graph to obtain multiple partitions (right).

distant, with an objective to preserve their relationships and encourage them to be clustered together. We introduce a simple cue to discover the similar saliency of those regions as the global connection measurement. We present a new energy function to partition the constructed graph, which formulates the minimization problem as a single and efficiently solvable eigenvector system. Based on the generated high quality graph partitions, we present an simple eigenvector histogram based representation to represent image regions and automatically drive effective unary potentials for the hierarchical random field of the Pylon model [14], yielding high-quality multi-class segmentation.

In brief, our proposed method exploits various simple and efficient cues to capture the high-level image information for segmentation. The cues are represented by a sophisticatedly connected graph yet with efficient graph partitioning capability. Compared with other state of the arts, our method significantly improves the segmentation efficiency and also achieves competitive performance. Sufficient experimental analyses on the BSDS500 image segmentation benchmark [9] demonstrate its effectiveness.

2. Related Works

Image segmentation has been studied in the computer vision community for decades. Shi *et al*. [4] propose normalized cuts (NCut), which advanced spectral clustering based image segmentation. Later, NCut is extended by [15] to multi-class segmentation. Many subsequent approaches have computed more effective affinity matrices using elaborately designed low-level features and metrics [3, 8, 9, 16]. To solve the limitation of NCut to capture affinities of distant pixels, several methods [6, 7, 16, 17] have been proposed base on multi-scaling affinity strategies.

Alternatively, Arbelaez *et al*. [9] propose the globalized probability of boundary (gPb), which utilizes the boundary-preserving characteristic of NCut with sophisticatedly designed features to detect object boundaries and incorporate it into the oriented watershed transform and ultrametric contour map (OWT-UCM) to conduct image segmentation. This approach becomes the main support of many subsequent segmentation approaches [18, 3, 19, 20, 10, 11]. Kim *et al*. [21] formulate a hypergraph-based model and perform correlation clustering for image segmentation. Recently, Yu *et al*. [5] minimize an ℓ_1-normed energy function of NCut to obtain piecewise smooth embeddings for gPb-owt-ucm [9], which obtains state-of-the-art image segmentation performance. However, all these methods suffer from expensive computations for feature extraction or optimization. Speed issues are considered in several following work. Multiscale combinatorial grouping (MCG) [10] segment images with multi-scale UCMs. Chen [11] provides a solution to the scale-alignment in MCG. On the other hand, Pont-Tuset *et al*. [22] propose a downsampled approximating algorithm to accelerate the graph partitioning and use richer information in multiscale UCMs. Tayor *et al*. [23] and many others [3, 21] reduce the size of the affinity matrix using superpixel techniques. In this paper, we developed an algorithm that is much faster than the aforementioned methods with competitive accuracies.

3. Global-local Connected Graph Partitioning

In this section, we present the approach to build the local and global connections of the graph. Then we introduce the proposed energy function to partition the constructed graph.

3.1. Local connection with co-occurrence cues

Our proposed method begins with an over-segmentation with a set of regions, defined as $\mathcal{S} = \{S_1, ..., S_N\}$. Denote the graph by $\mathcal{G}_{local} = \{\mathcal{S}, W\}$, where $W \in \mathbb{R}^{N \times N}$ is the affinity matrix with each entry W_{ij} representing the affinity between regions S_i and S_j. W is sparse such that only spatially adjacent region pairs within a small range have nonzero values. Given a test image with large appearance variations inside the object (see Figure 2), a desirable affinity matrix should be able to discover the strong affinity between two visually different neighboring regions belonging

to the common object.

One type of high-level knowledge comes from the fact that a neighboring region pair residing on an object is more likely to co-occur (i.e., have a high joint probability) due to the color patterns inside the object [18], such as the strip patten on the clothes of the images in Figure 2. If we treat regions $\{S_i|i = 1, ..., N\}$ as random variables, we can define the co-occurrence of two regions as

$$CO(S_i, S_j) = \log \frac{1}{A} P(S_i, S_j), \tag{1}$$

where $P(S_i, S_j)$ is the joint probability over S_j and S_j. Let $A = P(S_i)P(S_j)$ represent a normalization term, which is crucial to penalize the biased-high $P(S_i, S_j)$ of background region pairs against foreground object region pairs, because the background area usually has larger proportion than foreground objects. This normalization term will eliminate this unbalance accordingly. We estimate $P(S_i, S_j)$ and marginal distribution $P(S_i)$ by using a nonparametric kernel density estimator [24] following [18]. But differently, to learn the estimator, we densely sample region pairs of each region and its adjacent regions within a certain (i.e. e_1) distance apart without repetition.

Energy function: The first term E_{local} in our proposed energy function will encourage frequently co-occurring region pairs to be clustered into a group, and vice versa. Minimizing E_{local} is defined as the following:

$$\min_{\boldsymbol{y}} \sum_{i=1}^{N}\sum_{j=1}^{N} ||y_i - y_j||^2 W_{ij}, \quad s.t.\ \boldsymbol{y}^T D \boldsymbol{y} = 1, \tag{2}$$

where D is a diagonal matrix and its i-th diagonal element is $d_{ii} = \sum_j W_{ij}$. The constraint is the key to normalize the cut of the graph. $\boldsymbol{y} = [y_1, ..., y_N]^T$ is a real-valued vector, which is interpreted as a binary graph partition in NCut or a one dimensional embedding in Laplacian eigenmaps. W_{ij} is defined as

$$W_{ij} = \exp\left(\sum_o CO(S_i^{f_o}, S_j^{f_o})\right), \tag{3}$$

where the superscript f_o specifies a feature representation of the corresponding region. For each region, we calculate the pixel mean of Lab color space (f_1) and the diagonal values of the RGB color covariance matrix in a 3×3 window (f_2). W_{ij} is computed between S_i and S_j within e_2 ($e_2 > e_1$) distance apart.

3.2. Global connection with saliency cues

The graph associated with global connections is denoted by $\mathcal{G}_{global} = \{\mathcal{S}, K\}$. Our approach strengthens the locality-preserving character by discovering the underlying linear structures among spatially distant regions (i.e., each region can be linearly represented by several neighboring regions so that the global connections are directed) belonging to a common object, while these regions are adjacent on a certain manifold. This goal is achieved by minimizing the second energy term E_{global}:

$$\min_{\boldsymbol{y}} \sum_{i=1}^{N} ||y_i - \sum_{j \neq i} K_{ij} y_j||^2, \quad s.t.\ \boldsymbol{y}^T \boldsymbol{y} = 1, \tag{4}$$

where $K \in \mathbb{R}^{N \times N}$ is the coefficient matrix with R nonzero entries in each row to specify the linear combination coefficients of the representing neighbors. The constraint avoids degenerated solutions. $\boldsymbol{y}$ is interpreted as a one dimensional embedding in locally linear embedding (LLE) [25]. Note that both $\boldsymbol{y}$ and K are unknown; minimizing this energy function consists of three steps: 1) finding R neighbors for each region, 2) computing coefficient matrix K, and 3) computing $\boldsymbol{y}$.

Geodesic distance based neighbors: For each region, we consider its candidate neighbors from all regions within a large range of our defined geodesic distance, such that distance (s_{ij}) between regions S_i and S_j as

$$\begin{aligned} s_{ij} = \big(&\min(|w_{S_i} - w_{S_j}|, I_w - |w_{S_i} - w_{S_j}|)^2 \\ &+ \min(|h_{S_i} - h_{S_j}|, I_h - |h_{S_i} - h_{S_j}|)^2 \big)^{\frac{1}{2}}, \end{aligned} \tag{5}$$

where w_{S_i} and h_{S_i} denotes the spatial x- and y-coordinate of region S_i. I_w and I_h denote the width and height of the image, respectively. Intuitively, this metric treats the image as if it was wrapped along its four corners into a sphere and describes the geodesic distance along this resulting surface. The measurement can trace the connections of regions belonging to foreground objects or background with an arbitrary shape and range.

For a region S_i, we select R nearest regions with each region represented as a feature vector calculated by a saliency cue mapping σ. Then we find its coefficients K_i by

$$\begin{aligned} \min_{K_i} \ ||\sigma(S_i) - \sum_{j \neq i} K_{ij} \sigma(S_j)||^2 + \alpha\, \mathrm{tr}(K_i^T K_i), \\ s.t.\ \sum_j K_{ij} = 1. \end{aligned} \tag{6}$$

The regularization term is necessary to prevent ill-conditioned solutions when neighboring regions have similar feature values (i.e., making the Gram matrix singular). The regularization parameter is chosen as $\alpha = 1e{-}10$. The constraint ensures the translation invariance.

Saliency cue complying linearity: Spatially distant regions inside the same object may have large appearance variances, for example, the face, hairs, and clothes of a person exhibit totally different appearances (see Figure 2). Therefore, it is difficult to measure their latent similarity with traditional cues. Interestingly, those visually different

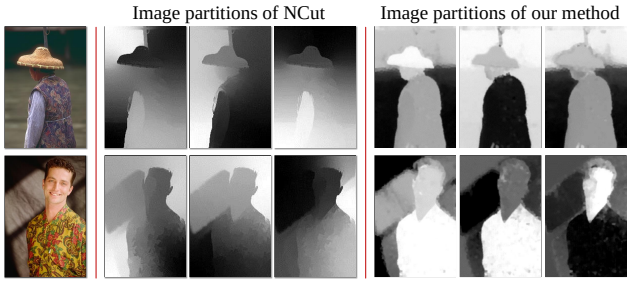

Figure 2: The graph partitioning results (the first three eigenvectors) of two sample images exhibiting large object internal appearance variances. NCut preserves edge information but segment images into connected components (middle). Our approach is able to separate the entire object from its background (right).

regions usually exhibit similar saliency degree in the human visual system [26, 27]. This characteristic remedies the "imperfection" of pairwise co-occurrence affinity and satisfies the requirement to build global connections. We take advantage of the empirical knowledge that salient objects in images have distinctive colors from the background under a certain linear combination of mixed color spaces [28]. To this end, we choose RGB, Lab, and hue and saturation channels of HSV (8 channels) and their nonlinear transformations with gamma correction (with three gamma values, $[0.5, 1.5, 2.0]$) to consider the human vision's nonlinear responses, thereby yielding a 24-dimensional feature vector for each region, $\sigma : \mathcal{S} \mapsto \mathbb{R}^{24}$.

Our method to incorporate saliency in the graph connection is elaborate. Unlike saliency detector [28], we do not compute the coefficient explicitly based on any supervised information. Since the correlation of each region feature vector $\sigma(S)$ is consistent under arbitrary linear transformation, its saliency characteristic between regions will be implicitly expressed in Eq. (4).

3.3. Proposed energy function to partition graph

Overall, the full graph we proposed is defined as $\mathcal{G} = \{\mathcal{S}, (W, K)\}$, where W specifies the local undirected connections and K specifies the global directed connections. Our goal is to pursue global partitioning of the graph $\mathcal{G}$, i.e., minimizing the two energy terms simultaneously. Therefore, the energy function E can be defined and derived as follows (detailed derivations are skipped):

$$\begin{aligned} E &= E_{local} + \mu E_{global} \\ &= \sum_{i=1}^{N}\sum_{j=1}^{N} ||y_i - y_j||^2 W_{ij} + \mu \sum_{i=1}^{N} ||y_i - \sum_{i \neq j} K_{ij} y_j||^2 \\ &= \boldsymbol{y}^T (D - W + \mu M)\boldsymbol{y}, \end{aligned} \tag{7}$$

where $(D-W) \in \mathcal{R}^{N \times N}$ is the Laplacian matrix and $M = (I-K)^T(I-K) \in \mathcal{R}^{N \times N}$. μ is a regularization parameter to balance E_{global} and E_{local}. Selecting the optimal value of μ is discussed in the experimental section.

It is easy to see that minimizing E is simply solving a generalized eigenvector system:

$$(D - W + \mu M)\boldsymbol{y} = \lambda D \boldsymbol{y}, \tag{8}$$

which produces a set of eigenvectors $\hat{Y}$, where each column is an eigenvector representing a binary partition of the graph. In practice, the number of segments of an arbitrary test image is unknown and the expected partition is not guaranteed to be the eigenvector associated with the second smallest eigenvalue [4]. In Section 4, we present a novel approach to address this issue for multi-class segmentation.

Leverage E_{local} and E_{gloal}: The two energy terms are designed for different purposes. E_{local} preserves the pairwise similarity of spatially adjacent region pairs, while E_{global} preserves the linear structure of spatially distant regions in the common object. Both emphasize the locality-preserving for the purpose of clustering (or graph partitioning). Compared with the hard constraint of E_{local}, E_{global} encourages a soft (i.e., likelihood) clustering of the regions [12]. In Figure 2, we visualize several graph partition results of our approach and compare it to NCut. As can be observed, the significantly improved graph partitioning quality demonstrates the effectiveness and necessity of the global connections introduced in E_{global}.

4. Multi-class Segmentation

In this section, we introduce the approach to use graph partitions for multi-class segmentation.

4.1. EigenHistogram

We have computed a set of eigenvectors (i.e., image partitions) $\hat{Y} = [\hat{\boldsymbol{y}}_1, ..., \hat{\boldsymbol{y}}_d] \in \mathbb{R}^{N \times d}$ corresponding to the first d smallest eigenvalues (excluding the zero eigenvalue) using Eq. (8). The i-th region can now be represented as a d-dimensional vector $S_i^{\hat{Y}}$. The k-means is applied to group regions into L segments, $\mathcal{Z} = \{\mathcal{Z}_k\}_{k=1}^{L}$, to produce a hard partition [3, 4]. To obtain more reliable multi-class segmentation, we treat it as a prior segmentation to provide the class likelihood for the multi-class segmentation. Note that our method can deal with the number of segments regardless of pre-defined L; we discuss this in the experiments.

For each dimension of $S_i^{\hat{Y}}$, we compute a histogram with L bins uniformly spaced between $[0, 1]$ based on the corresponding normalized eigenvector. As a consequence, a region will be represented as a $(d \times L)$-dimensional concatenated histogram (we use d=6 eigenvectors empirically and will discuss the parameter L in the experimental section). For each segment $\mathcal{Z}_k$, we accumulate and normalize the histograms of all regions belonging to this segment. We term this region representation as EigenHistogram (see Figure 3).

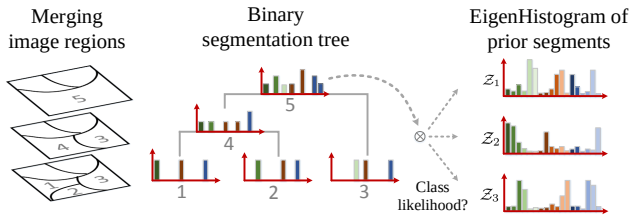

Figure 3: In the merged binary segmentation tree, each leaf node representing an initial image region has an EigenHistogram while the EigenHistograms of inner nodes are accumulated and normalized from that of their descendant nodes. Each node computes its class likelihood based on the EigenHistograms of the prior segmentation $\mathcal{Z}$.

4.2. Multi-class segmentation

EigenHistogram can be treated as a high-level representation which possesses spatial consistency, thereby intrinsically scalable to image segments of arbitrary size; furthermore, it is easy and fast to compute without any supervision as other methods [29, 14, 30] conduct. We will see that it is an very effective representation to compute the unary potentials of a hierarchical random field model.

Following the Pylon model [14], we can configure the regions into a hierarchical binary segmentation tree. Different from traditional "flat" random field models [31, 2], each node in our tree structure stands for a region nested from bottom to top, which enables the features to be extracted from different levels of the hierarchy to enrich the feature representation of the segments. In total, the constructed tree has $2{\cdot}N{+}1$ regions (the root node is the whole image), $\mathcal{S}^+ = \{S_i | i = 1, ..., 2{\cdot}N{+}1\}$, which define a hierarchical random field. We compute the unary potential of region S_i assigned to the k-th segment as:

$$U_{p_i=k} = -\beta \cdot \langle \mathcal{H}(S_i), \mathcal{H}(\mathcal{Z}_k) \rangle, \; S_i \in \mathcal{S}^+, \; \mathcal{Z}_k \in \mathcal{Z}, \quad (9)$$

where U_{p_i} is the unary potential of the region $S_i \in \mathcal{S}^+$ to specify the cost of assigning label p_i to S_i. β determines the weight of the unary potential against the pairwise potential. $\mathcal{H}$ transforms a region into the EigenHistogram representation, where the class likelihood is calculated for each region in the tree. Following [14], we compute the pairwise potentials as the exponentiated boundary strength.

EigenHistograms of the internal nodes of the binary segmentation tree are accumulated and normalized from that of the corresponding descendant nodes (see Figure 3). Therefore, the partial non-smoothness effects of the eigenvectors (i.e., isolated regions as visualized in the right panel of Figure 2) reflected in the EigenHistograms of top-level nodes will be suppressed. We can leave the rest computation to the whole inference procedure to produce a holistic multi-class segmentation as the final output.

Table 1: Segmentation results and runtime comparison on BSDS500.

Method	Covering		PRI		VoI		Time(s)
	ODS	OIS	ODS	OIS	ODS	OIS	
NCut [4]	.45	.53	.78	.80	2.23	1.89	-
Felz-Hutt [1]	.52	.57	.80	.82	2.21	1.87	-
Mean Shift [32]	.54	.58	.79	.81	1.85	1.64	-
ISCRA [33]	.59	.66	.82	.85	1.60	1.42	30
gPb-owt-ucm [9]	.59	.65	.83	.85	1.69	1.48	240
cPb-owt-ucm [3]	.59	.65	.83	.86	1.65	1.45	>240
red-spectral [23]	.56	.62	.83	.85	1.78	1.56	∼12
DC-Seg [20]	.58	.63	.82	.85	1.75	1.59	6
DC-Seg$_{\text{full}}$ [20]	.59	.64	.82	.85	1.68	1.54	144
PMI$_{\text{low}}$ [18]	.61	.66	.83	.86	1.58	1.42	30*
MCG [10]	.61	.66	.83	.86	1.57	1.39	18
PFE+ucm [5]	.61	.66	.83	.86	1.64	1.46	>900·$b^\dagger$
PFE+MCG [5]	.62	.68	.84	.87	1.56	1.36	>900·$b^\dagger$
Ours	.62	.66	.83	.86	1.59	1.43	9

*Time is tested on half size images. $^\dagger b{=}\{4, 8, 16\}$ is the number of the embedding needs to compute.

5. Experimental Results

We evaluate the proposed segmentation approach using the challenging Berkeley Segmentation Dataset (BSDS500) [9]. BSDS500 is widely used as the benchmark for image segmentation and boundary detection, which contains 200 training, 100 validation, and 200 test images. We use several standard evaluation criteria [9] to conduct quantitative analysis: Segmentation Covering, Probability Rand Index (PRI), and Variation of Information (VoI) with the optimal dataset scale (ODS) and the optimal image scale (OIS).

5.1. Implementation details

We investigate the parameter sensitivity of our method and select the optimal values based on the training set, and apply these values to the totally independent test set.

Figure 4 shows the performance with respect to L for k-means clustering, R for Eq. (6), μ for graph partitioning. The parameter of L is fully dependent on the test set, but we choose not to rely on the test set to select the best L, with the purpose to demonstrate the strong generalization ability of the proposed method. For parameter μ, compared with $\mu = 0$, which means only E_{local} are considered in the energy function, E_{global} ($\mu = 8$) improves the accuracy by $>$.1ODS (Covering). More importantly, we observe .2ODS improvement ($\mu = 0$ vs. $\mu = 8$) on the test set (see the last row of Table 3), which indicates the effectiveness of our proposed E_{global}. As can be observed, our method is insensitive to the three parameters. In practice, we set $L = 6$, $\mu = 8$, and $R = 14$ throughout following experiments.

We empirically set $e_1 = 20$ for kernel density estimation in Eq. (1) and $e_2 = 40$ for W computation in Eq. (3). Since the test set has approximately equal image sizes, we can assume that these two values can be generalized to all test images. We empirically found that the parameter of β in Eq. (9) varies from images to images. In practice, we run the inference procedure to obtain multiple segmentations by

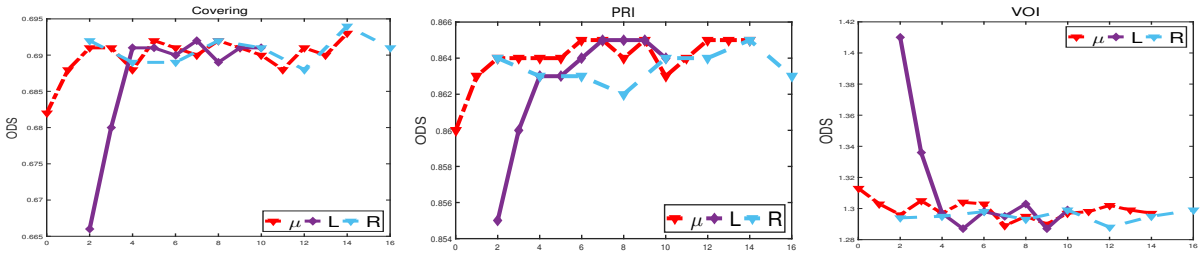

Figure 4: The parameter sensitivity evaluation of the proposed method by varying parameters on the training dataset. From left to right: evaluation scores of Covering, PRI and VOI with respect to L, R and μ, as indicated in x-axis. It can be observed that our method is insensitive to the parameters.

Table 2: The running time (in second) of each phase of our method.

Phase	Mean	Max	Mean	Var.
1: Region structure generation	2.60	3.73	3.08	0.05
2: Graph construct. and partition	3.30	6.89	4.51	0.56
3: Multi-class segmentation	1.39	2.26	1.71	0.03
Total	7.54	12.6	9.30	1.00

varying the β value between $[200, 300, ..., 800]$ with an interval equal to 100, and take the average of all these outputs and the superpixel map as the final segmentation.

We use the toolbox provided by Dollár *et al*. [34] to generate the superpixel map (i.e., structured edge (SE) detector followed by UCM) with roughly uniform region sizes. Our implementation is based on Matlab running on a standard Intel i7 desktop.

5.2. Segmentation result comparison

In Table 1, we compare the proposed approach to several state-of-the-art methods in terms of segmentation accuracy and running time on the BSDS500 test set. As one can see, our method significantly outperforms most of the comparative methods. PMI_{low} [18] is a boundary detection method, which embeds the edge map into OWT-UCM [9] to obtain accurate segmentation. Its best accuracy is achieved on a low resolution version. The recently proposed multiscale combinatorial grouping (MCG) [10] and piecewise flat embedding (PFE) obtain significant improvement compared with the early methods. MCG uses hierarchical UCMs to boost the performance. PFE integrates its computed embeddings into the gPb-owt-ucm [9] and MCG, which achieves good segmentation performance. However, PFE suffers from the computationally expensive optimization. Our proposed method outperforms PEF+owt-ucm and achieves close segmentation performance compared with PFE+MCG. More importantly, our method is hundreds of times faster than PFE based methods. DC [20] and red-spectral [23] also emphasize on fast image segmentation, but their segmentation accuracy is not as accurate as ours.

Figure 5 shows the qualitative segmentation results. The last column presents one graph partitioning result of our method, which provides good initial segmentation proposals. Compared with other methods, our approach is able to resist the object internal variances to avoid small segments, so that the segmentations are much more spatially consistent. In addition, our method can implicitly figure out the best number of segments regardless of the pre-defined $L = 6$. It is because EigenHistogram can penalize the over-segmentation since homogeneous segments will have similar EigenHistogram and thus proximate unary potentials, encouraging them to be merged. The first three rows of Figure 5 particularly highlight above mentioned capability.

Table 3: Segmentation results using different region generation baselines indicated in $(\cdot)$. Please see text for explanation of different configurations. The last row is the result of our method (SE+ucm) when E_{global} is not applied.

Method	Covering		PRI		VoI	
	ODS	OIS	ODS	OIS	ODS	OIS
SemiContour+ucm	.56	.63	.82	.85	1.79	1.57
Ours (SemiC.+ucm)	.60	.64	.83	.85	1.68	1.50
MCG	.61	.66	.83	.86	1.57	1.39
Ours (MCG)	.62	.66	.84	.86	1.57	1.40
SE+ucm	.59	.64	.83	.86	1.71	1.51
Ours (SE+ucm)	.62	.66	.83	.86	1.59	1.43
Ours, w/o E_{global}	.60	.65	.83	.85	1.64	1.44

Efficiency: The comparison of running time is shown in the rightmost column of Table 1. The image size for testing is 321×481. Our proposed method is much faster than most algorithms because of several important designs:

1. Our method needs none complex feature computation.
2. We construct the graph model based on superpixels rather than raw pixels. Although we incorporate multiple cues into a graph with complicated constraints, the graph partitioning is a single eigenvector system.
3. EigenHistogram is efficient to compute and very scalable to regions with arbitrary size for hierarchical multi-class segmentation.

We also evaluate the detailed running time on the total 200

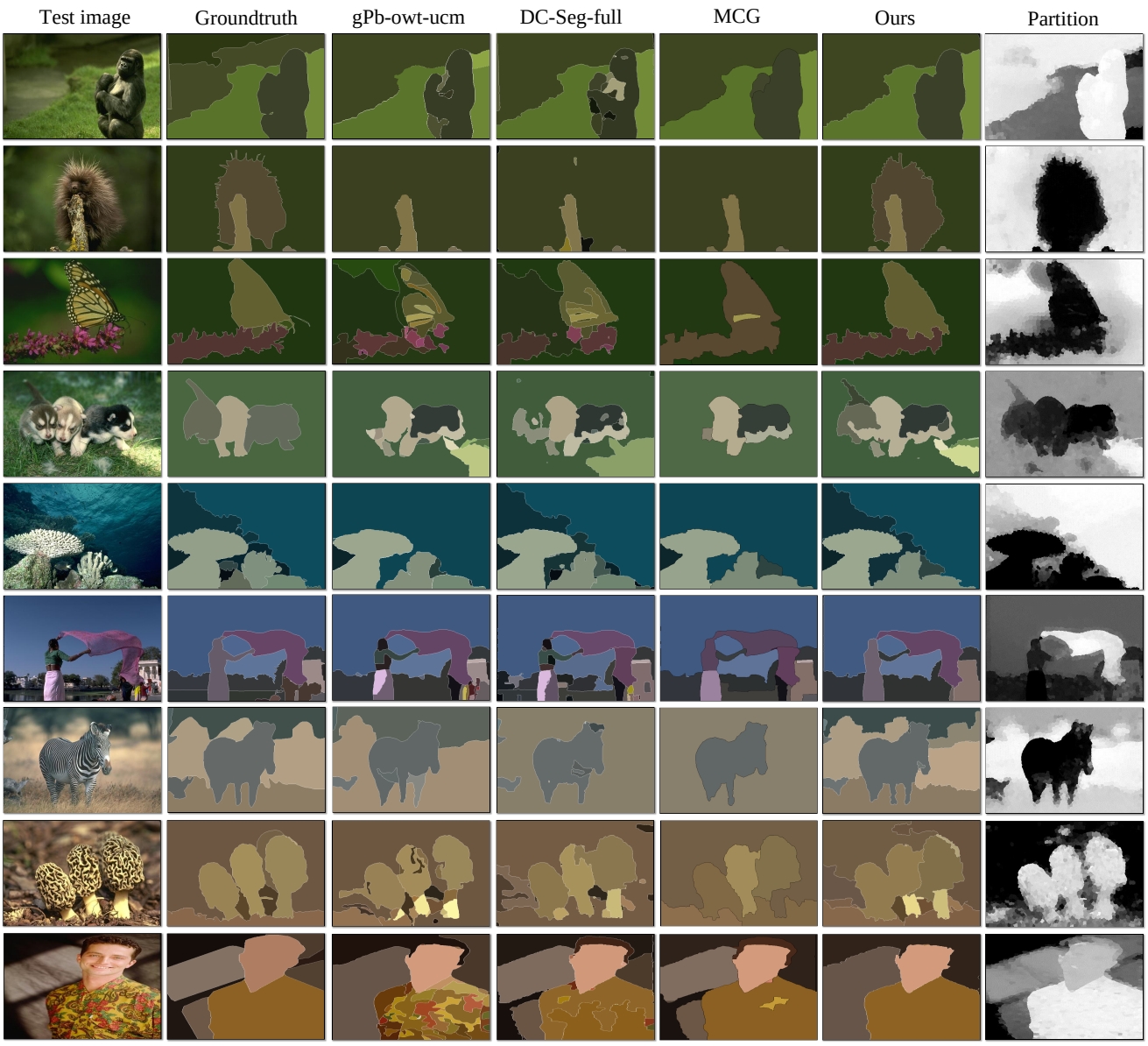

Figure 5: Segmentation results on BSDS500. The first and second columns show the test images and the ground truth, respectively. The next three columns show the results of gPb-owt-ucm [9], DC-Seg$_{\text{full}}$ [20], MCG [10] and our method, and these results are visualized with the optimal scale (ODS) of corresponding methods used for quantitative evaluation. The last column presents one graph partition result of our method.

test images. Our method is executed in three phases: 1) generating superpixel map and constructing the hierarchical segmentation tree, 2) constructing and partitioning the graph, and 3) conducting multi-class segmentation. Table 2 shows the detailed time cost of each phase. Compared with most comparative methods, our proposed approach is more scalable for practical usages.

5.3. Analysis

We consider the cases of using different methods to generate superpixel maps as the input of our method, which allow us to conduct more detailed analyses. It is necessary to notice that, although our method is quite flexible to build upon these methods, it is not an extension of underling methods. In contract, the proposed method is a new exploration of accurate and fast spectral clustering based image segmentation.

In addition, many state-of-the-art methods use accurate supervised edge detector and other trained classifiers [10, 11]. We are particularly interesting in reducing training data demand towards completely unsupervised image segmentation. Either unsupervised [35] or semi-supervised

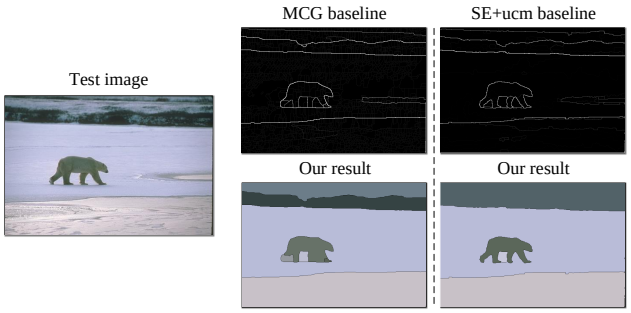

Figure 6: Segmentation results using MCG and SE+ucm to generate superpixel map for our method. MCG sharpens noisy edges below the bear (upper left), resulting in worse segmentation.

SE detector [36] can be used as our underlying edge detectors. We consider using the latter, namely SemiContour [36] (3 BSDS training images are used), as an alternative to the originally used SE. We compare the performance in Table 3. Our segmentation consistently improves the segmentation accuracy of baseline methods. Particularly, we observe significant .4ODS (Covering) improvement over SemiContour+ucm and .3ODS improvement over SE+ucm.

Edge information: The improvement using MCG as the baseline is a small margin (i.e., .1ODS) compared with cases of using other two as baselines. In fact, MCG uses SE to detect edges while it also sharpens edges. Nevertheless, we observe MCG sometimes sharpens irrelevant edges as well, such that the sharpened noisy edges will have a large penalization through pairwise potentials against unary potentials in our multi-class segmentation procedure, leading to undesirable results. Figure 6 illustrates this situation. The above results indicate that our segmentation relies less on strong edge information compared with MCG.

Additionally, since our method relies less on edges, one potential weakness of our graph partitioning is the fragmentation of homogeneous regions, which decreases the precision of the boundary detection. We compare the boundary precision-recall curve in Figure 7. Our method maintains nearly the same precision with the baseline methods, i.e., MCG and SE+ucm (though negligibly 0.03 decrease for SE+ucm).

Strengths and limitations: The proposed method is fairly effective in discovering complex image knowledge from challenging natural images to segment objects even for objects that have weak boundaries. The proposed algorithm is significantly better than MCG in those samples shown in Figure 8(left). However, we found that the proposed algorithm is not proficient at images without definite objects, because our graph design emphasizes the high-level discriminative image knowledge of objects against the background. MCG outperforms ours in those samples (see Figure 8(right)). In addition, MCG is applied onto large-scale

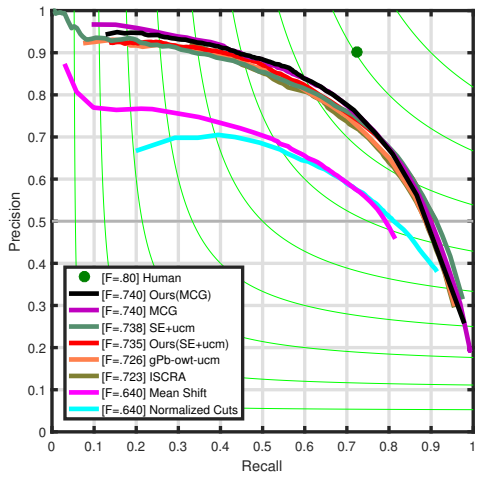

Figure 7: Precision-Recall curves for boundaries on BSDS. $(\cdot)$ shows the baseline method used by our method.

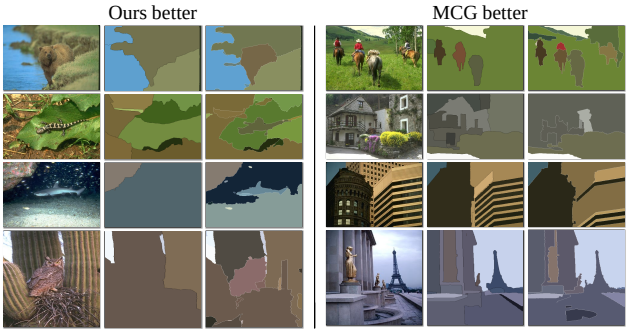

Figure 8: Sample results of our method with SE+ucm baseline (right) and MCG (middle) [10].

PASCAL object segmentation and proposal tasks. We leave unsupervised large-scale segmentation as future work .

6. Conclusions

In this paper, we present a fast yet accurate image segmentation method, which is a novel re-examination of spectral clustering based image segmentation for unsupervised image segmentation. We construct an image region graph with both local and global connections based on simple but effective high-level cues, and formulate the graph partitioning as a simple generalized eigenvector system. The high quality graph partitions are used to compute effective unary potentials of Pylon model for multi-class image segmentation. Sufficient experiments on the BSDS benchmark show that the proposed method achieves significantly faster speed and competitive performance with many state of the arts.

References

[1] P. F. Felzenszwalb and D. P. Huttenlocher, "Efficient graph-based image segmentation," *IJCV*, vol. 59, no. 2, pp. 167–

181, 2004. 1, 5

[2] Y. Boykov, O. Veksler, and R. Zabih, "Fast approximate energy minimization via graph cuts," *PAMI*, vol. 23, no. 11, pp. 1222–1239, 2001. 1, 5

[3] T. H. Kim, K. M. Lee, and S. U. Lee, "Learning full pairwise affinities for spectral segmentation," *PAMI*, vol. 35, no. 7, pp. 1690–1703, 2013. 1, 2, 4, 5

[4] J. Shi and J. Malik, "Normalized cuts and image segmentation," *PAMI*, vol. 22, no. 8, pp. 888–905, 2000. 1, 2, 4, 5

[5] Y. Yu, C. Fang, and Z. Liao, "Piecewise flat embedding for image segmentation," in *ICCV*, pp. 1368–1376, 2015. 1, 2, 5

[6] S. X. Yu, "Segmentation induced by scale invariance," in *CVPR*, pp. 444–451, 2005. 1, 2

[7] M. Maire and S. X. Yu, "Progressive multigrid eigensolvers for multiscale spectral segmentation," in *Proceedings of the IEEE International Conference on Computer Vision*, pp. 2184–2191, 2013. 1, 2

[8] T. Cour, F. Benezit, and J. Shi, "Spectral segmentation with multiscale graph decomposition," in *CVPR*, pp. 1124–1131, 2005. 1, 2

[9] P. Arbelaez, M. Maire, C. Fowlkes, and J. Malik, "Contour detection and hierarchical image segmentation," *PAMI*, vol. 33, no. 5, pp. 898–916, 2011. 1, 2, 5, 6, 7

[10] P. Arbelaez, J. Pont-Tuset, J. Barron, F. Marques, and J. Malik, "Multiscale combinatorial grouping," in *CVPR*, pp. 328–335, 2014. 1, 2, 5, 6, 7, 8

[11] Y. Chen, D. Dai, J. Pont-Tuset, and L. Van Gool, "Scale-aware alignment of hierarchical image segmentation," 2016. 1, 2, 7

[12] M. Belkin and P. Niyogi, "Laplacian eigenmaps for dimensionality reduction and data representation," *Neural computation*, vol. 15, no. 6, pp. 1373–1396, 2003. 1, 4

[13] A. Y. Ng, M. I. Jordan, Y. Weiss, *et al.*, "On spectral clustering: Analysis and an algorithm," vol. 2, pp. 849–856, 2002. 1

[14] V. Lempitsky, A. Vedaldi, and A. Zisserman, "Pylon model for semantic segmentation," in *NIPS*, pp. 1485–1493, 2011. 2, 5

[15] S. X. Yu and J. Shi, "Multiclass spectral clustering," in *ICCV*, pp. 313–319, 2003. 2

[16] Z. Li, X.-M. Wu, and S.-F. Chang, "Segmentation using superpixels: A bipartite graph partitioning approach," in *CVPR*, pp. 789–796, 2012. 2

[17] X. Wang, Y. Tang, S. Masnou, and L. Chen, "A global/local affinity graph for image segmentation," *Image Processing, IEEE Transactions on*, vol. 24, no. 4, pp. 1399–1411, 2015. 2

[18] P. Isola, D. Zoran, D. Krishnan, and E. H. Adelson, "Crisp boundary detection using pointwise mutual information," in *ECCV*, pp. 799–814, 2014. 2, 3, 5, 6

[19] R. Xiaofeng and L. Bo, "Discriminatively trained sparse code gradients for contour detection," in *NIPS*, pp. 584–592, 2012. 2

[20] M. Donoser and D. Schmalstieg, "Discrete-continuous gradient orientation estimation for faster image segmentation," in *CVPR*, pp. 3158–3165, 2014. 2, 5, 6, 7

[21] S. Kim, C. D. Yoo, S. Nowozin, and P. Kohli, "Image segmentation using higher-order correlation clustering," *PAMI*, vol. 36, no. 9, pp. 1761–1774, 2014. 2

[22] J. Pont-Tuset, P. Arbelaez, J. T. Barron, F. Marques, and J. Malik, "Multiscale combinatorial grouping for image segmentation and object proposal generation," *arXiv preprint arXiv:1503.00848*, 2015. 2

[23] C. J. Taylor, "Towards fast and accurate segmentation," in *CVPR*, pp. 1916–1922, 2013. 2, 5, 6

[24] E. Parzen, "On estimation of a probability density function and mode," *The annals of mathematical statistics*, pp. 1065–1076, 1962. 3

[25] S. T. Roweis and L. K. Saul, "Nonlinear dimensionality reduction by locally linear embedding," *Science*, vol. 290, no. 5500, pp. 2323–2326, 2000. 3

[26] M. Cheng, N. J. Mitra, X. Huang, P. H. Torr, and S. Hu, "Global contrast based salient region detection," *PAMI*, vol. 37, no. 3, pp. 569–582, 2015. 4

[27] A. Borji, D. N. Sihite, and L. Itti, "Salient object detection: A benchmark," in *ECCV*, pp. 414–429, 2012. 4

[28] J. Kim, D. Han, Y.-W. Tai, and J. Kim, "Salient region detection via high-dimensional color transform," in *CVPR*, pp. 883–890, 2014. 4

[29] J. Yang, Y.-H. Tsai, and M.-H. Yang, "Exemplar cut," in *ICCV*, pp. 857–864, 2013. 5

[30] C. Farabet, C. Couprie, L. Najman, and Y. LeCun, "Learning hierarchical features for scene labeling," *PAMI*, vol. 35, no. 8, pp. 1915–1929, 2013. 5

[31] V. Kolmogorov and R. Zabin, "What energy functions can be minimized via graph cuts?," *PAMI*, vol. 26, no. 2, pp. 147–159, 2004. 5

[32] D. Comaniciu and P. Meer, "Mean shift: A robust approach toward feature space analysis," *PAMI*, vol. 24, no. 5, pp. 603–619, 2002. 5

[33] Z. Ren and G. Shakhnarovich, "Image segmentation by cascaded region agglomeration," in *CVPR*, pp. 2011–2018, 2013. 5

[34] P. Dollár and C. Zitnick, "Fast edge detection using structured forests," *PAMI*, 2015. 6

[35] Y. Li, M. Paluri, J. M. Rehg, and P. Dollár, "Unsupervised learning of edges," *CVPR*, 2016. 8

[36] Z. Zhang, F. Xing, X. Shi, and L. Yang, "Semicontour: A semi-supervised learning approach for contour detection," *CVPR*, 2016. 8